

# Green and reusable Ag/AgCl-TiO<sub>2</sub> nanocomposites for visible light-triggered dye degradation

Mohammadreza Maneshi<sup>1</sup>, Pierfrancesco Cerruti<sup>2\*</sup>, Arash Moeini<sup>3</sup> and Mansooreh Davoodi<sup>1,4\*\*</sup>

<sup>1</sup>Institute for Color Science and Technology, Tehran, Iran

Eliminato: <sup>1</sup>Iran Polymer and Petrochemical Institute

<sup>2</sup>Institute for Polymers, Composites and Biomaterials (IPCB-CNR), Via Campi Flegrei 34, 80078 Pozzuoli, Italy

<sup>3</sup>Fluid Dynamics of Complex Biosystems, School of Life Sciences Weihenstephan, Technical University of Munich 85354 Freising, Germany

<sup>4</sup>Department of Chemistry, Science and Research Branch, Islamic Azad University, Tehran, Iran.

Eliminato: <sup>4</sup> Department

\* Correspondence: Pierfrancesco Cerruti

Affiliation: Institute for Polymers, Composites and Biomaterials (IPCB-CNR), Via Campi Flegrei 34, 80078 Pozzuoli, Italy.

Email Address: cerruti@ipcb.cnr.it

Eliminato: E-mail

\*\* Co-Correspondence: Mansooreh Davoodi

Affiliation: Department of Chemistry, Science and Research Branch, Islamic Azad University, Tehran, Iran.

Eliminato: E-mail Address: [m\\_davoodi67@yahoo.com](mailto:m_davoodi67@yahoo.com)

Email Address: [davoodi-mn@icrc.ac.ir](mailto:davoodi-mn@icrc.ac.ir)

Formattato: Colore carattere: Automatico

Arash Moeini, email: [arash.moini@tum.de](mailto:arash.moini@tum.de)

Formattato: Interlinea: multipla 1,15 ri

Mohammadreza Maneshi, email: [maneshi-mr@icrc.ac.ir](mailto:maneshi-mr@icrc.ac.ir)

Formattato: Colore carattere: Automatico

Mansooreh Davoodi, email: [davoodi-mn@icrc.ac.ir](mailto:davoodi-mn@icrc.ac.ir)

Eliminato: mohammadreza.maneshi@yahoo.com

**Abstract:** Ag/AgCl-TiO<sub>2</sub> plasmonic nanocomposites (NCs) are endowed with excellent visible-light photocatalytic activity. However, only a few studies investigated environmentally friendly approaches to their synthesis. In this work, Ag/AgCl-TiO<sub>2</sub> NCs at five different compositions were prepared in a single-step process by a green and cost-effective route, using *Satureja khuzistanica Jamzad* aqueous extract. The role of the aqueous plant extract as a reducing and stabilizing agent, and the formation of the NCs was evidenced by several techniques, including FT-IR, EDS, SEM, HRTEM, elemental mapping, and XRD. The morphological analysis demonstrated that the NCs formed nanoaggregates with an average size of 30 nm. The synthesized Ag/AgCl-TiO<sub>2</sub> NCs displayed a remarkable photoactivity in the visible light region, as confirmed by the significantly higher degradation rates of methyl orange (MO) compared to TiO<sub>2</sub>. In particular, the 15% Ag/TiO<sub>2</sub> molar ratio

Formattato: Colore carattere: Automatico

Eliminato: m\_davoodi67@yahoo.com

Formattato: Colore carattere: Automatico

Eliminato: have an

Eliminato: their

Eliminato: ,

Eliminato: nanocomposites

Eliminato: different

Eliminato: showed a nanoaggregate arrangement of NCs,

Eliminato: A remarkable increase of photoactivity of the

Eliminato: was

Eliminato: displayed by all synthesized nanocomposites

Eliminato: sample with a

sample revealed a MO degradation efficiency higher than 99% under visible light, and retained high photocatalytic activity even after several degradations runs. Overall, the green, cost-effective, and scalable synthesis of Ag/AgCl-TiO<sub>2</sub> NCs herein reported provides a novel, more sustainable strategy for the high-efficiency modification of TiO<sub>2</sub> photocatalyst in engineering and other environmental applications.

**Keywords:** Ag/AgCl-TiO<sub>2</sub> nanocomposites; Green synthesis; photocatalysis; Surface plasmonic vibration; Water purification

## 1. Introduction

Titanium dioxide (TiO<sub>2</sub>) nanoparticles (NPs) have a wide range of properties, such as easy availability, low price, photo-corrosion stability, low toxicity, and appropriate bandwidth range. Therefore, they are broadly used as biosensors, gas, and chemical oxygen demand (COD) sensors [1]. In addition, the TiO<sub>2</sub> NPs photocatalytic activity under sunlight or ultraviolet irradiation yields highly active materials with high oxidation power, which can eliminate a large part of organic contamination, or can be used in photovoltaic cells, electrochromic devices, and polymer-based nanocomposites [2].

The TiO<sub>2</sub> bandgap (3.2 V for anatase and 3 V for rutile) requires UV light for excitation. However, since less than 5% of the solar radiation falls in the UV spectrum, TiO<sub>2</sub> should be chemically modified in order to adjust its bandgap, thus allowing to increase absorption in the visible region [3]. For this purpose, various strategies have been undertaken, such as metal coupling [4–10], or bonding to non-metallic elements [11,12] and materials that are sensitive to visible light [13,14]. Doping with anions or cations is a viable strategy for extending TiO<sub>2</sub> spectral response to the visible region and improving its photocatalytic activity [3,15]. This approach enables a more significant portion of the solar energy spectrum to be absorbed, and creates a charge trap for electron-hole separation [16]. However, doping makes these materials unstable and corrosive, and doping levels are difficult to control [17]. Silver halides are commonly used to address this issue [18–22], as although they are unstable under sunlight, they can be used as highly stable photocatalysts when mixed with TiO<sub>2</sub> [23].

Eliminato: displayed more than 99%

Eliminato: retaining

Eliminato: degradation

Eliminato: potential

Eliminato: use

Eliminato: results in the production of

Eliminato: ,

Eliminato: can be

Eliminato: is made of

Eliminato: the

Eliminato: needs to be adjusted

Eliminato: allow absorption

Eliminato: for better photocatalytic properties [3].

Eliminato: for TiO<sub>2</sub> optimization

Eliminato: approach

Eliminato: improve

Eliminato: using

Eliminato: larger

Eliminato: ,

Eliminato: for solving

Eliminato: problem

Eliminato: and

Several methods have been reported for synthesizing Ag/AgX-TiO<sub>2</sub> (X=F, Cl, Br, I) nanocomposites (NCs) [6,7,24–27]. However, the synthesis process of the heterogeneous Ag/AgCl-TiO<sub>2</sub> structure is not straightforward, often involving time-consuming, multi-stage methods. Also, the reported single-step methods typically use organic solvents and chemicals which are not environmentally friendly, and possibly harmful to health [25]. All the mentioned reasons pushed scientists to find novel eco-friendly pathways for synthesizing Ag/AgCl-TiO<sub>2</sub> NCs [28–34].

Plants are the primary source of active compounds such as polyphenols, terpenoids, tannins, alkaloids, and polyketides. These compounds can be potentially used in the biosynthesis of Ag/AgCl-TiO<sub>2</sub> NCs as reducing agents of metal cations as well as stabilizers of the final products [35–38]. In this regard, *Satureja khuzistanica* Jamzad is one of the species of the *Satureja* genus. This wild plant is known as “Marze” and has a geographical distribution in the western, northern, and southern Iran regions, particularly in the southwestern Zagros Mountains, where is known as a natural healing agent with antiseptic and analgesic properties [39]. The phytochemical analysis evidenced the presence of rosmarinic acid, flavonoids, and terpenoids in *S. kuzistanica* aerial parts [40–42]. Several studies reported that flavonoids and terpenoids can be suitably used as metal-reducing agents [35,36,38,43]. On this basis, the present study aimed to develop an eco-friendly, simple, reproducible, and cost-effective method to replace the conventional chemical processes for synthesizing Ag/AgCl-TiO<sub>2</sub> NCs with high photocatalytic activity in the visible region. In particular, an *S. kuzistanica* extract was used to synthesize Ag/AgCl-TiO<sub>2</sub> NCs at varying Ag/TiO<sub>2</sub> ratios. The resulting NCs were then thoroughly characterized in their chemical, morphological, and photocatalytic properties, using methyl orange (MO) dye as a model pollutant.

## 2. Materials and Methods

### 2.1. Reagents

Eliminato: and  
Eliminato: involves  
Eliminato: , which is very time-consuming.  
Eliminato: ,  
Eliminato: the synthesis of

Eliminato: spices  
Eliminato: , a  
Eliminato: which  
Eliminato: commonly  
Eliminato: “,  
Eliminato: part of the  
Eliminato: . *S. khuzistanica*  
Eliminato: used  
Eliminato: curing  
Eliminato:

Eliminato: methods  
Eliminato: a  
Eliminato: with

AgNO<sub>3</sub>, methyl orange (Mw: 327.33), and NaCl (99% pure) were purchased from Merck. TiO<sub>2</sub> nanoparticles (P25 Evonik) were used in the NCs preparation procedure.

Eliminato: Methyl Orange

Eliminato: )

## 2.2. Preparation of plant extract

The plant material of *Satureja khuzistanica* Jamzad was collected from Khorraman Pharma Co. (Khorramabad, Iran) in June 2019. Dr. Javad Hadian has identified the plant material (voucher specimen MPH-1582) at Shahid Beheshti University, Tehran.

Then, 50 g of the dried and powdered aerial parts of *S. khuzistanica* were mixed with 100 ml of double-distilled water and stirred by a magnetic stirring heater at 80 °C for 60 min. The extract was filtered and centrifuged at 7,000 rpm and room temperature, and then stored in the fridge for subsequent treatment.

Eliminato: kuzistanica was

Eliminato: then

Eliminato: heating stirrer

Eliminato: prepared

## 2.3. Synthesis of silver NPs using *S. khuzistanica* extract

1.26 mmol of silver nitrate salt (AgNO<sub>3</sub>) solution 0.1 M was added to 20 mL of deionized water and stirred for 10 min. The *S. khuzistanica* extract was added to the solution under stirring. The formation of Ag NPs could be seen visually by the change of the solution color from pale yellow to reddish-brown.

## 2.4. Single-step synthesis of Ag/TiO<sub>2</sub> nanocomposite

TiO<sub>2</sub> (1.0 g) NPs were added to 10 ml of double-distilled water and mixed well. Then, 0.62 mmol of AgNO<sub>3</sub> 0.1 M was added to the mixture at 75 °C under stirring. After 10 min, *S. khuzistanica* extract (8 ml) was added dropwise to the mixture under stirring. The final solution changed color from white to dark brown when heated. Next, the suspension was mixed well using a magnetic stirrer at 300 rpm and 75 °C for 10 minutes. The particles were then collected after centrifugation of the solution for 10 minutes at 8,000 rpm and room temperature. Finally, the nanocomposite was rinsed two times with ethanol and then dried at 50 °C overnight in a vacuum oven.

Eliminato: Satureja

Eliminato: while stirred.

Eliminato: showed a

Eliminato: change

Eliminato: it was

Eliminato: The

Eliminato: then

Eliminato: Finally, the

Eliminato: for 10 minutes and

Eliminato: by

Eliminato: ,

Eliminato: during the night

Eliminato: the

## 2.5. Single-step synthesis of Ag/AgCl-TiO<sub>2</sub> nanocomposite

In order to synthesize Ag/AgCl-TiO<sub>2</sub> nanocomposites, Ag and AgCl-doped TiO<sub>2</sub> NPs were prepared by the dropwise addition of five different mole percentage ratios of Ag ions (2%, 5%, 10%, 15%, 20%) to a TiO<sub>2</sub> dispersion (TiO<sub>2</sub> (2 g) in 8 ml of deionized water) under stirring at 75 °C (Table 1). Subsequently, different volumes (1.6, 4, 8, 12, and 16 ml) of *S. khuzistanica* extract were added. As soon as the color changed from white to dark brown, NaCl's same mole ratio as Ag<sup>+</sup> was added to each batch, and the stirring continued for another 10 min at 75 °C. The precipitated particles were collected by centrifugation at 8,000 rpm for 10 minutes and rinsed two times with ethanol. Finally, the nanocomposites were dried overnight in a vacuum oven at 50 °C. In a preliminary investigation by this method, five batches of Ag/AgCl-TiO<sub>2</sub> NCs (S1-S5) with different mole percentage ratios of Ag/TiO<sub>2</sub> were synthesized (Figure 1 and Table 1). Among them, sample S4 evidenced the best results in terms of photocatalytic activity. Therefore, S4 (Ag/AgCl-TiO<sub>2</sub> nanocomposite with a 15% Ag/TiO<sub>2</sub> mol ratio) was selected for further characterization.

Eliminato: into

Eliminato: After that

Eliminato: was

Eliminato: in

Eliminato: the

Eliminato: .

Eliminato: , in this paper

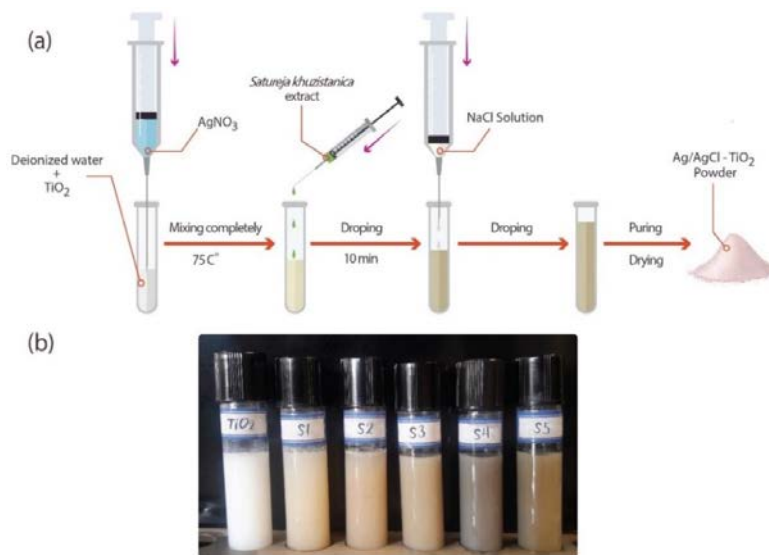


**Figure 1.** (a) Schematic of the synthesis process of the Ag/AgCl-TiO<sub>2</sub> NC photocatalysts, (b) Synthesized NCs and TiO<sub>2</sub> dispersed in water.

Eliminato: for hierarchical

**Table 1.** Synthesized NC samples with the corresponding Ag/TiO<sub>2</sub> molar and weight ratios.

Sample	Ag/TiO <sub>2</sub> ratio (mol%)	Ag/TiO <sub>2</sub> ratio (wt%)
S1	2	2.7
S2	5	6.7
S3	10	13.5
S4	15	20.3
S5	20	27

Eliminato: Samples

Eliminato: (

Formattato: Non Apice / Pedice

Eliminato: (

Tabella formattata

## 2.6. Structural and morphological characterization

Fourier transform infrared spectroscopy (FT-IR) spectra were acquired by a Thermo Nicolet NEXUS 870 spectrophotometer (USA) in transmission mode, with a resolution of 4 cm<sup>-1</sup> and 16 scans. The

UV-visible spectra were recorded using a double-beam Hitachi U-2900 spectrophotometer in the range of silver absorption (300-600).

Eliminato: (Hitachi)

Eliminato: at a

Eliminato: range

Morphology and scattering of the particles were explored using scanning electron microscopy-electron dispersive spectroscopy (SEM-EDX) by means of an FEI ESEM QUANTA 200 (USA) on powder

Eliminato: The morphological structure

Formattato: Giustificato

Eliminato: particle

samples. Elemental analysis was performed with an EDX system (EDAX Genesis EDS Detector) coupled to the SEM. The sample was placed on conductive adhesive tape and coated with a 10 nm thick

Eliminato: a

Eliminato: ),

Eliminato: EDAX Genesis

layer of Au-Pd alloy. Transmission electron microscopy (TEM) and a high-resolution TEM (HRTEM) were performed using a 100-kV Philips EM208S and a Tecnai G2 F20 S-Twin TEM devices, respectively.

Eliminato: an

Eliminato: slice

For this purpose, the samples were dispersed in ethanol, sonicated, collected on a copper grid (400 mesh) coated with carbon film, and dried.

Eliminato: ),

Eliminato: ,

Eliminato: and dried

X-ray diffraction (XRD) of the NCs was measured using a Seifert XRD 3003 X-RAY diffraction device.

The X-ray step size was 0.01°, and XRD patterns were measured over a 20-80° 2θ range, with a scanning rate of 2°/min. The average crystalline size (D) was calculated by the Scherrer equation, using the Origin Pro software.

$$D = \frac{K\lambda}{\beta \cos\theta}$$

Where K = 0.94, λ = 0.154 nm, β = half width of the diffraction band (FWHM) and θ = Bragg diffraction angle.

### 2.7. Investigation of the Ag/AgCl-TiO<sub>2</sub> NCs visible light photoactivity

An aqueous solution of methyl orange (MO) dye (Figure 2) was used to assess the photocatalytic performance of Ag/AgCl-TiO<sub>2</sub> nanocomposite in the visible light region. Three UV-filtered 4W warm white SMD-LED lamps (3750 Lux) (λ > 400 nm) provided the visible light source. All of the experimental procedures were carried out at room temperature. First, 50 mg of Ag/AgCl-TiO<sub>2</sub> sample were added to 24.5 ml of water and stirred for 60 min. Next, the resulting mixture was sonicated for 5 min (Bandelin Sonoplus HD 2070). Then, 0.5 ml of 500 mg/L MO solution were added to the suspension in the dark and stirred for about 35–60 min. Finally, the suspensions containing photocatalyst and dye molecules were irradiated with visible light for 24 hours and then centrifuged two times at 10000 rpm for 5 min for the complete separation of solids. Then, the supernatant transparent solution's absorption spectra were measured at 300-600 nm wavelength using a Hitachi U-2900 UV-Vis spectrophotometer. This process was repeated for all five synthesized NCs (S1-S5) and TiO<sub>2</sub> samples [25]. For each sample, the methyl orange (MO) concentration was determined from the absorption peak, and the percent photocatalytic degradation was calculated using the following equation (Figure 7).

Eliminato: equal to

Eliminato: 01°,

Eliminato: at

Eliminato: of 2θ (20-80)

Eliminato: ,

Eliminato:  $\frac{K\lambda}{\beta \cos\theta}$

Eliminato: width

Eliminato: figure

Eliminato: region of

Eliminato: Warm

Eliminato: LUX

Eliminato: completed

Eliminato: samples

Eliminato: The

Eliminato: minutes

Eliminato: L

Eliminato: a

Eliminato: room

Eliminato: treated under the

Eliminato: were

Eliminato: the

Eliminato: of 300-600 nm

Eliminato: spectrophotometer (

Eliminato: ,

Eliminato: -

Eliminato: -

Eliminato: ). The methyl orange (MO) concentrations were determined from the absorption peak.

Eliminato: After that,

Eliminato: sample's

Eliminato: rate

Eliminato: through

Eliminato: Table 2

$$\text{Degradation (\%)} = (1 - (A_s/A_b)) \times 100$$

Where  $A_b$  is the blank sample (MO) absorption, and  $A_s$  is the sample's absorption. The sample S4 was reused up to five times after the first photocatalysis cycle, by recovering and filtering the NC suspension containing the degraded MO and repeated washing with DI water.

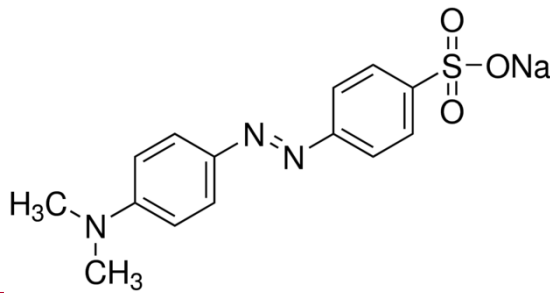


Figure 2. Methyl Orange (MO) chemical structure.

### 3. Results and discussion

According to previous studies, several polyphenol compounds, including flavonoids like rosmarinic acid, taxifolin, and 7-methoxy luteolin, might be responsible for the chemical reduction of metal ions in the synthesis of NCs [41,42,44]. Therefore, according to the presence of similar compounds in *S. khuzistanica* extract, the latter was used as a reducing agent of  $\text{Ag}^+$  in this work. The synthesis of silver NPs using *S. khuzistanica* extract was monitored by UV-Vis spectroscopy. The absorption spectrum of the synthesized Ag NPs in the visible region displayed a peak at 448 nm, related to a plasmonic vibration on the Ag NPs surface [45]. Although the reduction mechanism ascribed to the extract has not been reported in the literature, the most likely route, including some of the redox reactions involving the phenolic constituents of the extract, is shown in Figure 3 [46].

Eliminato: absorption of the

Eliminato: of the sample

Eliminato: ,

Eliminato: ¶

Eliminato: ¶

Formattato: Allineato al centro

Eliminato:

Eliminato: such as

Eliminato: Taxifolin

Eliminato: metal

Eliminato: due

Eliminato: extract

Eliminato: investigated

Eliminato: silver nanoparticles

Eliminato: silver nanoparticles'

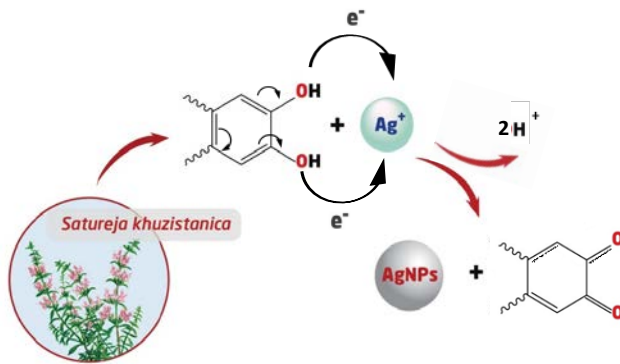


Figure 3. Proposed mechanism for the formation of the Ag NPs using *S. khuzistanica* extract.

### 3.1. Chemical characterization of the NCs

FT-IR spectroscopy was employed to detect specific functional groups of the extract and the synthesized NPs. As shown in Figure 4, the FT-IR spectra allowed to rationalize the role of *S. khuzistanica* extract as a reducing agent by identifying the functional groups of compounds such as flavonoids, terpenoids, caffeic acids, and tannins [47]. These compounds, particularly flavonoids and terpenoids, might reduce their activity by converting phenol groups to aldehydes and carboxylic acids [43]. Indeed, in the FT-IR spectrum of the *S. khuzistanica* aqueous extract (Figure 4a), the broad peak at 3000 to 3500  $\text{cm}^{-1}$  is attributed to the stretching vibrations of the hydroxyl groups of phenolic compounds [48]. In addition, the peak at 1412  $\text{cm}^{-1}$  corresponds to phenolic C–OH stretching vibration [12,48,49]. The other relevant peaks that confirmed the presence of flavonoids, triterpenoids, and polyphenols, were at 790 and 893  $\text{cm}^{-1}$ , belonging to C–Cl and methyl group ( $\text{CH}_3$ -) stretching, 1261  $\text{cm}^{-1}$  attributed to C–O stretching, the amide I peak observed at 1635  $\text{cm}^{-1}$ , the peak at 2925  $\text{cm}^{-1}$  correlated to methyl C–H asymmetric or symmetric stretching, and finally the peaks at 3435, and 3743  $\text{cm}^{-1}$  attributed to phenols (O–H group), alcohol, carboxylic acid, and carbonate ion

Eliminato: The

Eliminato: technique

Eliminato: investigate the presence of

Formattato: Normale, Allineato a sinistra

Eliminato: it is

Eliminato: rationalized

Eliminato: the identification of

Eliminato: In

Eliminato: spectra

absorption frequencies [47,48,50,51]. Several studies pointed out that amide groups and polyphenols can reduce metal nanoparticles, also acting as stabilizing agents for NCs [38,52,53]. In this respect, Ghasemi et al. used a mangrove tree extract to synthesize Ag/AgCl-TiO<sub>2</sub> NCs. They proposed that the plant extract's role as a reducing and stabilizing agent for the synthesis of NCs might be due to flavonoids and terpenoids [54]. In TiO<sub>2</sub> spectra (Figure 4b), the 530–710 cm<sup>-1</sup> bands are related to Ti–O stretching vibrations [55]. The framework vibration band of Ti–O/Ti–O–Ti was observed at 632 cm<sup>-1</sup> [48]. The broad absorptions at 3440 cm<sup>-1</sup> were ascribed to OH stretching [56], and the peak at 1631 cm<sup>-1</sup> is associated with the O–H bending vibrations of the absorbed water molecules [57]. The formation of NCs was confirmed by a broad peak at 818 cm<sup>-1</sup> observed in both Ag/TiO<sub>2</sub> and Ag/AgCl-TiO<sub>2</sub>, attributed to the stretching vibrations fitting the metal-oxygen bonds like M–O or O–M–O (M = Ti or Ag) (Figure 4c and d) [30,58]. In addition, the broad band from 450 to 1025 cm<sup>-1</sup> shifted to a higher wavelength in NCs in comparison with the blank TiO<sub>2</sub>, which might be due to the presence of Ag and Ti atoms and the mixing of Ag–O and Ti–O at the molecular level in the nanocomposite (Figure 4c and d) [54]. However, the presence of Ag in nanocomposites is hard to be noticed by FT-IR spectroscopy, because the Ag–O stretching band overlapped with Ti–O vibration [30,55,58,59].

Eliminato: bands in the

Eliminato: range

Eliminato: and 1631

Eliminato: and

Formattato: Evidenziato

Formattato: Evidenziato

Eliminato: modes

Formattato: Evidenziato

Formattato: Evidenziato

Formattato: Evidenziato

Eliminato: Ti-OH, respectively [56,

Formattato: Colore carattere: Rosso, Evidenziato

Formattato: Colore carattere: Rosso

Eliminato: –

Eliminato: attributed

Eliminato: ,

Formattato: Evidenziato

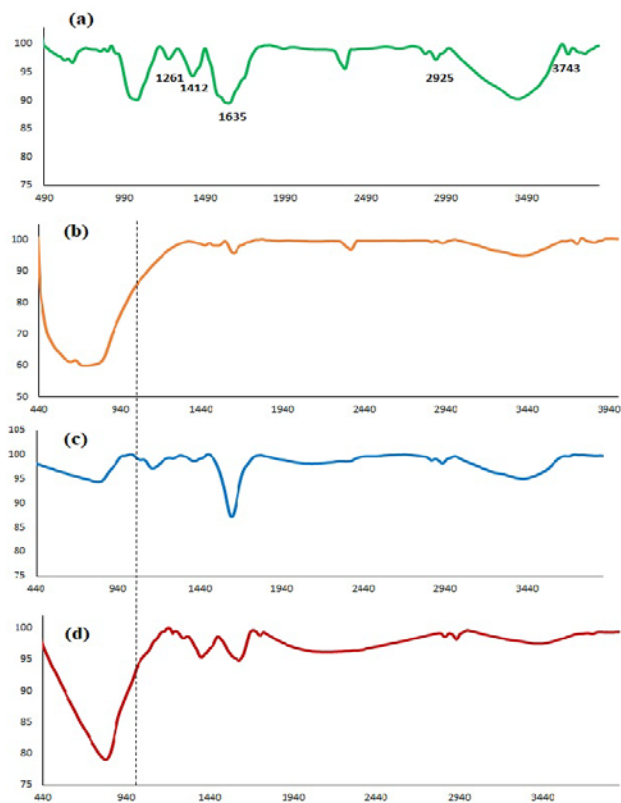


**Figure 4.** Transmission FT-IR spectra of (a) *Satureja khuzistanica* aqueous extract, (b) TiO<sub>2</sub>, (c) TiO<sub>2</sub>/Ag, (d) Ag/AgCl-TiO<sub>2</sub> (sample S4).

Eliminato :

### 3.2. Visible light-triggered photocatalytic activity of the NCs

The optical properties of the photocatalytic NCs in this study were proved and compared by methyl orange (MO) dye degradation tests (Figure 5) using visible spectroscopy. The purpose of the synthesis of the Ag/AgCl-TiO<sub>2</sub> nanocomposites is to enhance the photocatalytic performance of TiO<sub>2</sub> in the visible light range, so warm white SMD-LED lamps (3750 LUX) ( $\lambda > 400$  nm) were used as a visible light source.

Formattato: Colore carattere: Nero

Eliminato: promote

Formattato: Colore carattere: Automatico

The role of Ag NPs in Ag/AgCl-TiO<sub>2</sub> NCs should be considered to elucidate the methyl orange (MO) degradation mechanism. Indeed, the Surface Plasmon Resonance (SPR) effect of Ag NPs improves the local inner electromagnetic field and enhances visible light absorption [6,20,60,61].

Eliminato: To illustrate the methyl orange (MO) degradation mechanism, the

Eliminato: into

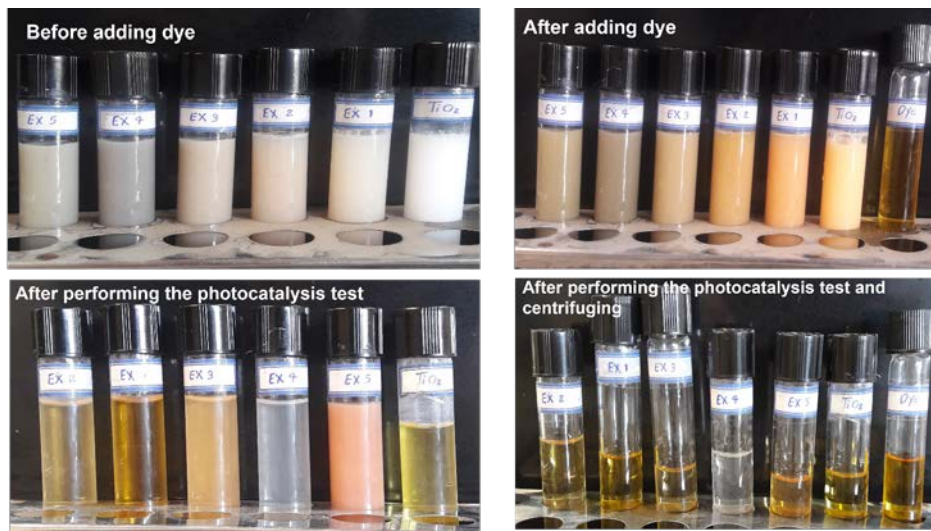


Figure 5. The visible appearance of the MO dye degradation tests of the Ag/AgCl-TiO<sub>2</sub> NCs.

Eliminato: Visible

As shown in Figure 6, the excited electrons emitted from the plasmon-excited Ag NPs could shift to both the Conduction Band (C<sub>B</sub>) of TiO<sub>2</sub> and AgCl at the Ag/TiO<sub>2</sub> and Ag/AgCl interface [62]. In the case of Ag/AgCl-TiO<sub>2</sub> NCs, due to the less negative conduction band (C<sub>B</sub>) edge of TiO<sub>2</sub> (-0.10 V vs. NHE) compared to AgCl (-1.2 V vs. NHE), the excited electrons are conducted to the C<sub>B</sub> of TiO<sub>2</sub> instead of AgCl [63]. Therefore, photoexcited electrons could shift from AgCl and Ag C<sub>B</sub> to TiO<sub>2</sub> C<sub>B</sub>, trapped there by the excitation of O<sub>2</sub> and other oxidative agents to O<sub>2</sub><sup>-</sup> and/or ·OH<sub>2</sub> that are mainly responsible for the MO degradation [6,64]. On the other hand, a hole shifts from the Ag Valence Band (V<sub>B</sub>) to AgCl because the negative charge could induce the oxidation of Cl<sup>-</sup> ions to Cl radical with high

Eliminato: interface

Eliminato: were

Eliminato: main

Eliminato: shifted

Eliminato: of

oxidation ability [22,61]. The chlorine radical could then oxidize the MO dye, thereby restoring chloride ions (Figure 6) [65]. It is to underline that the thorough elucidation of the degradation mechanism and the main active species during the photocatalytic degradation of MO would require ESR experiments.

Eliminato: so the Cl radical could be reduced to

Eliminato: again

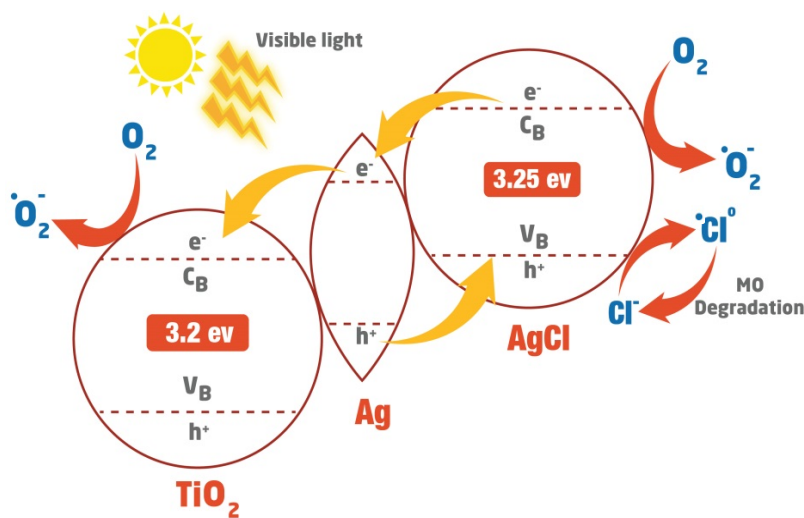


Figure 6. Photocatalytic mechanisms of Ag/AgCl-TiO<sub>2</sub> under visible light.

Eliminato: -

Formattato: Colore carattere: Automatico

To evaluate the MO degradation rate, the absorption peak of MO at 464 nm was measured in all five NC samples (S1-S5) and TiO<sub>2</sub> nanoparticles after irradiation under visible light for 24 h (Figure 7a). The results evidenced that the photocatalytic activity of S4 was remarkably higher than that measured for the other samples, while about 25% MO degradation was noted for undoped TiO<sub>2</sub>. This was likely due to the optimal amount of Ag, which could adequately improve the dynamical electron transfer between Ag and TiO<sub>2</sub>, and reduce the electron-hole recombination in Ag/AgCl/TiO<sub>2</sub> [27]. Indeed, the NCs' photocatalytic activity directly depends on the amount of Ag NPs interacting with TiO<sub>2</sub>, principally because transferring electrons from these non-contact Ag NPs to TiO<sub>2</sub> can be

Eliminato: result

Eliminato: is

Eliminato: also reducing

Eliminato: the transfer of

very challenging [25]. Indeed, the accumulation of Ag NPs inhibits light absorption and decreases photocatalytic activity [25]. In other words, in Ag/TiO<sub>2</sub> system, the transfer of the electrons from the Ag NPs to the C<sub>B</sub> of TiO<sub>2</sub> can corrode the Ag nanoparticles and induce the formation of Ag<sup>+</sup>, making this system unstable [63]. Therefore, AgCl<sub>2</sub> as the third component in the Ag/AgCl-TiO<sub>2</sub> triple nanocomposite<sub>2</sub> prevents the photo corrosion of the nanoparticles and the oxidation of silver ions, improving the stability of the whole system [64]. The studies concluded that Ag/AgX-TiO<sub>2</sub>, X (F, Cl, Br, I) is a highly stable photocatalyst when irradiated by visible light, and the silver halides are easily decomposed, forming silver metal when exposed to light [65,66].

Eliminato: which makes

Eliminato: resulting in

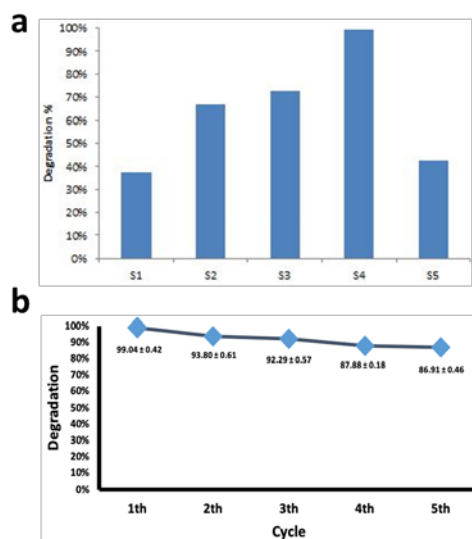


**Figure 7.** (a) Percent degradation rate of MO by using five different samples of Ag/AgCl-TiO<sub>2</sub> NCs; (b) Photocatalytic stability of S4 (reported values correspond to the mean ± standard deviation, n=3.)

These photocatalysts were reusable after simple filtering and washing with DI water. In particular, the photocatalytic stability of S4, with an Ag/TiO<sub>2</sub> molar ratio of 15%, was monitored. The result showed that S4 could maintain high visible-light photocatalytic activity even after five successive runs (each cycle lasted 24 h under visible light) (Figure 7b).

Eliminato: a

Eliminato: of MO degradation

Eliminato: the fifth

Eliminato: run

### 3.3. Structural and morphological analysis of the Ag/AgCl-TiO<sub>2</sub> NCs

Since S4 (the Ag/AgCl-TiO<sub>2</sub> nanocomposite with a 15% Ag/TiO<sub>2</sub> mol ratio) yielded the best results

regarding photocatalytic activity, the latter was selected to carry out a more detailed structural and morphological characterization. By studying the XRD pattern of the Ag/TiO<sub>2</sub> NP sample (Figure 8b),

the diffraction peaks of the TiO<sub>2</sub> anatase phase defined by T could be observed (Figure 8a, JCPDS file

no: 21-1272) [67]. The other peaks at  $2\theta = 37.3^\circ$  and  $62.2^\circ$  (labeled with A) are attributed to the Ag cubic phase (JCPDS file no: 65-2871) [68]. In the S4 XRD pattern, other peaks at  $2\theta$  of  $27.2^\circ$ ,  $31.8^\circ$ ,

$45.7^\circ$ ,  $54.6^\circ$ ,  $57.1^\circ$ ,  $68.4^\circ$ , and  $74.6^\circ$  (identified with C) are associated with AgCl crystal cubic phase

(JCPDS no. 85-1355) [69] (Figure. 8c). According to a previous study, other small peaks might be associated with the diffraction of impurities or other phases such as Ag<sub>x</sub>O, which were hard to be identified [54].

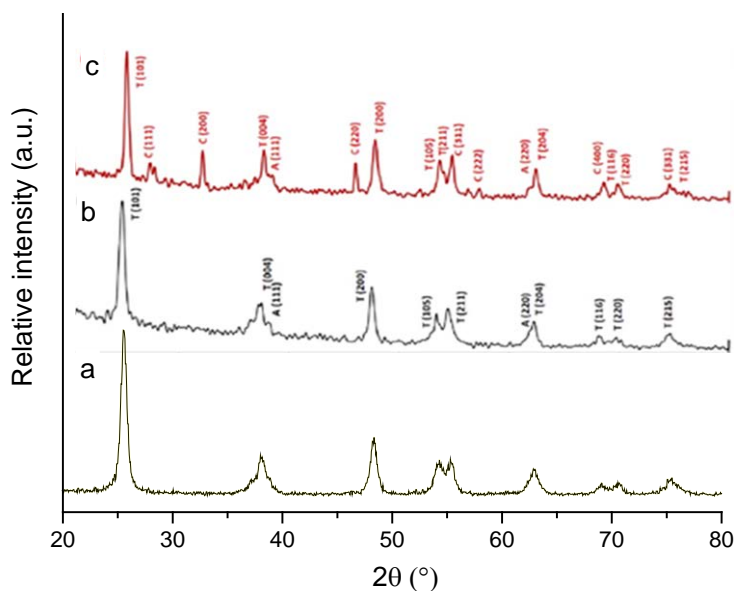


Figure 8. XRD patterns of: (a) anatase TiO<sub>2</sub>, (b) Ag/TiO<sub>2</sub> NPs, and Ag/AgCl-TiO<sub>2</sub> NPs (sample S4).

Eliminato: ¶

Eliminato: in terms of

Eliminato: for

Eliminato: further

Eliminato: marked

Eliminato: ,

Eliminato: to

Eliminato: )

Eliminato:

Using the Scherrer equation, full width at half maximum (FWHM) and average crystalline size (D) of Ag/AgCl-TiO<sub>2</sub> NCs particles were obtained from the XRD patterns. As shown in Table 2, Ag/AgCl-TiO<sub>2</sub> NCs particle sizes were 19 to 37 nm, with an average size of 22 nm.

Eliminato: From

Eliminato: XRD patterns, the

Eliminato: was measured, using

Eliminato: Scherrer equation

Eliminato: particles size

Eliminato: in the range of

**Table 2.** FWHM and average crystalline size (D) of Ag/AgCl-TiO<sub>2</sub> NC particles.

peak position (2θ, °)	FWHM	size(nm)
24.9	0.43	19.8
31.0	0.23	37.9
45.8	0.26	34.4
47.6	0.57	15.9
53.6	0.79	11.7
62.4	0.735	13.2

Tabella formattata

EDX analysis of S4 provided elemental identification of Ag/AgCl-TiO<sub>2</sub> NCs. As shown in Figure 9a, the atomic percentages of O, Ti, Ag, and Cl elements of S4 were 61.17, 32.87, 3.88, and 2.09, respectively. Given the atomic percentages of Cl and Ag in the sample, it might be that not all silver ions were converted to AgCl, and both Ag<sup>0</sup> and AgCl were simultaneously present. The atomic percentage of Cl was due to AgCl NPs, and the percentage of Ag was related to Ag<sub>2</sub> and AgCl NPs formed on TiO<sub>2</sub>. The two times higher percentage of oxygen to Ti indicated the TiO<sub>2</sub> existence. The atomic ratio of Ag to Ti was 11.8, slightly lower than the nominal Ag/TiO<sub>2</sub> ratio reported in Table 1 (15%), indicating that about 20% of the added AgNO<sub>3</sub> did not react, and was washed out in the purification steps.

Eliminato: close to

Eliminato: stoichiometry mole percentage

Eliminato: .

Elemental mapping images investigated the element scattering in Ag/AgCl-TiO<sub>2</sub> NPs (S4). The result showed that Ag and AgCl nanoparticles were homogeneously distributed on the surface of TiO<sub>2</sub> NP-aggregates (Figure 9b).

Eliminato: nanoparticles

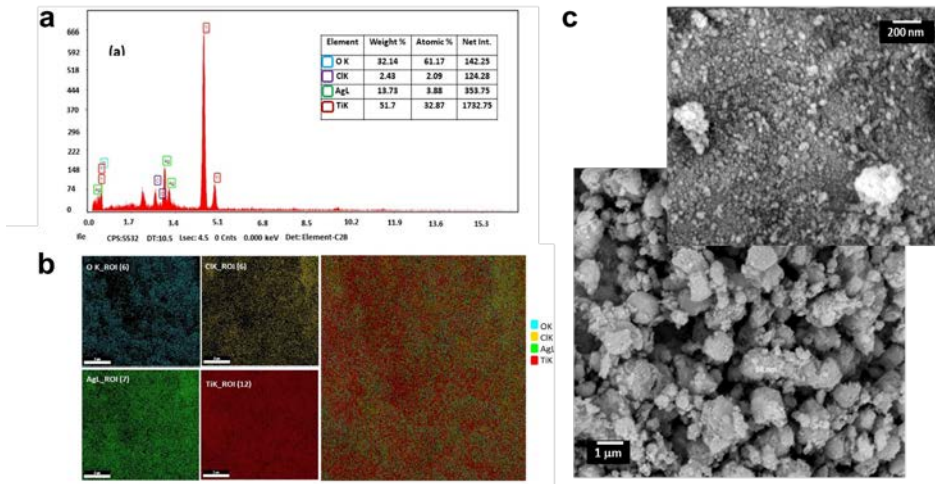


**Figure 9.** (a) EDX spectrum, (b) EDX elemental mapping, and (c) Field Emission Scanning Electron Microscopy (FESEM) image of S4.

The SEM images of S4 showed a particulate morphology, with roughly spherical particles having sizes on the order of micrometers (Figure 9c). However, higher magnification image demonstrated that the latter were constituted by aggregated primary nanosized particles of about 20 nm. This finding was in accordance with the XRD results and indicated that the formation of micron-sized particles takes place by an aggregative nucleation and growth mechanism occurring during the synthesis process, as known for conductive nanocomposites [70].

The particle size and the morphological arrangement of Ag/AgCl-TiO<sub>2</sub> nanocomposites were further studied using TEM microscopy (Figure 10a). The dimensional analysis of the TEM morphograph of S4 indicated an average size of nanoparticles of about 35 nm, in accordance with the data gathered by SEM and XRD (Figure 10e)).

AgCl, Ag, and TiO<sub>2</sub> crystal planes were observed in a high-resolution TEM morphograph of the S4 sample (Figure 10b). The lattice distance of 0.23 nm was attributed to the (111) plane of cubic Ag,

Eliminato: with

Eliminato: as is noted by the

Eliminato: ,

Eliminato: made up

Eliminato: the aggregation of

Eliminato: nanostructured

Eliminato: ,

Eliminato: in size

Eliminato: were

Eliminato: 71

Eliminato: by

0.32 nm was related to the (111) plane of cubic AgCl, and 0.35 nm was associated with the (101) plane of TiO<sub>2</sub> anatase. Thus, the measured lattice spacing from different regions further corroborated the formation of the nanocomposite structure. Figure 10c displays the selected area electron diffraction (SAED) pattern of Figure 10b, and the diffraction rings are related to the different diffraction planes of TiO<sub>2</sub>, AgCl, and Ag crystals. Finally, high-angle annular dark-field (HAADF) images enabled to clearly distinguish silver-containing structures (Ag<sup>0</sup> and AgCl) from Ti, because a heavy element such as Ag gives a bright image contrast. In contrast, a lighter element such as Ti gives a gray image contrast (Figure 11d) [54,71].

Eliminato: to

Eliminato: nanocomposites

Eliminato: allow distinguishing

Eliminato: ,

Eliminato: , while

Eliminato: light

Eliminato: 110d

Eliminato: 72,73

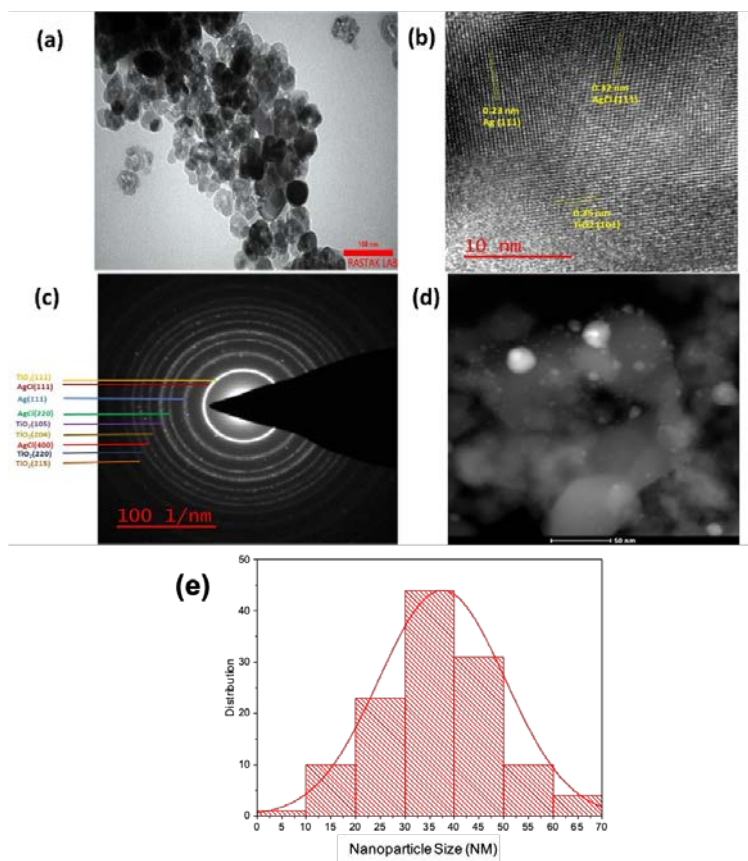


**Figure 10.** (a) Bright-field TEM, (b) HRTEM, (c) SAED pattern, (d) HAADF-STEM, and (e) average nanoparticles size distribution histogram of S4 NCs.

#### 4. Conclusion

A single-step process was developed to synthesize environmentally friendly plasmonic Ag/AgCl-TiO<sub>2</sub> nanocomposites, using a green and safe technique, solely using *Satureja khuzistanica* Jamzad aqueous extract as a reducing and stabilizing agent. The plant extract's role was confirmed by the presence of peaks of flavonoids, triterpenoids, and polyphenols in FT-IR spectra. In addition, several NC

Eliminato:

Eliminato: via the

Eliminato: , without using any organic solvent

Eliminato: Several NCs

formulations at different Ag/TiO<sub>2</sub> molar ratios were successfully prepared, showing remarkable catalytic activity in the visible-light triggered degradation of methyl orange.

Eliminato: successively

Eliminato: which showed

XRD, SEM, and TEM observations revealed the nanoaggregate morphology of the NCs, with primary particles having an average size of about 25 nm. Besides, elemental mapping of the sample showed an even distribution of Ag and AgCl NPs on the surface of TiO<sub>2</sub>. Furthermore, Ag nanoparticles' surface plasmonic resonance effect on the visible-light absorption evidenced that Ag NPs play a crucial role in improving TiO<sub>2</sub> photocatalytic performance by significantly increasing the photocatalyst activity and stability. Indeed, the Ag/AgCl-TiO<sub>2</sub> nanocomposite with a nominal 15% Ag/TiO<sub>2</sub> molar ratio exhibited outstanding performance, as it degraded 99% MO after 24 h visible-light irradiation, while retaining high photocatalytic activity even after five degradation runs.

Eliminato: ,

Eliminato: and retained

The green and easily scalable synthetic route of Ag/AgCl-TiO<sub>2</sub> NCs described here provides a feasible approach for preparing high-efficiency TiO<sub>2</sub>-based photocatalysts in engineering and environmental applications.

Eliminato: the preparation of

**Conflicts of Interest:** The authors declare no conflict of interest.

## References

- [1] J. Bai, B. Zhou, Titanium Dioxide Nanomaterials for Sensor Applications, Chem. Rev. 114 (2014) 10131–10176. <https://doi.org/10.1021/cr400625j>.
- [2] M. Ussia, A. Di Mauro, T. Mecca, F. Cunsolo, G. Nicotra, C. Spinella, P. Cerruti, G. Impellizzeri, V. Privitera, S. C. Carroccio, ZnO-pHEMA nanocomposites: an ecofriendly and reusable material for water remediation, ACS Appl. Mater. Interfaces 10 (2018) 40100-40110. <https://doi.org/10.1021/acsami.8b13029>.

- [3] S.G. Kumar, L.G. Devi, Review on Modified TiO<sub>2</sub> Photocatalysis under UV/Visible Light: Selected Results and Related Mechanisms on Interfacial Charge Carrier Transfer Dynamics, *J. Phys. Chem. A*. 115 (2011) 13211–13241. <https://doi.org/10.1021/jp204364a>.
- [4] X. Chen, H. Zhu, J.-C. Zhao, Z.-F. Zheng, X.-P. Gao, Visible-Light-Driven Oxidation of Organic Contaminants in Air with Gold Nanoparticle Catalysts on Oxide Supports, *Angew. Chem. Int. Ed. Engl.* 47 (2008) 5353–5356. <https://doi.org/10.1002/anie.200800602>.
- [5] J. Choi, H. Park, M.R. Hoffmann, Combinatorial doping of TiO<sub>2</sub> with platinum (Pt), chromium (Cr), vanadium (V), and nickel (Ni) to achieve enhanced photocatalytic activity with visible light irradiation, *J. Mater. Res.* 25 (2010) 149–158. <https://doi.org/10.1557/JMR.2010.0024>.
- [6] J. Yu, G. Dai, B. Huang, Fabrication and Characterization of Visible-Light-Driven Plasmonic Photocatalyst Ag/AgCl/TiO<sub>2</sub> Nanotube Arrays, *J. Phys. Chem. C*. 113 (2009) 16394–16401. <https://doi.org/10.1021/jp905247j>.
- [7] J. Zhang, X. Liu, X. Suo, P. Li, B. Liu, H. Shi, Facile synthesis of Ag/AgCl/TiO<sub>2</sub> plasmonic photocatalyst with efficiently antibacterial activity, *Mater. Lett.* 198 (2017) 164–167. <https://doi.org/https://doi.org/10.1016/j.matlet.2017.04.029>.
- [8] C. Zhang, H. Hua, J. Liu, X. Han, Q. Liu, Z. Wei, C. Shao, C. Hu, Enhanced Photocatalytic Activity of Nanoparticle-Aggregated Ag–AgX(X = Cl, Br)@TiO<sub>2</sub> Microspheres Under Visible Light, *Nano-Micro Lett.* 9 (2017) 49. <https://doi.org/10.1007/s40820-017-0150-8>.
- [9] Y. Zhao, R. Li, L. Mu, C. Li, Significance of Crystal Morphology Controlling in Semiconductor-Based Photocatalysis: A Case Study on BiVO<sub>4</sub> Photocatalyst, *Cryst. Growth Des.* 17 (2017) 2923–2928. <https://doi.org/10.1021/acs.cgd.7b00291>.
- [10] J. Zhu, S. Pang, T. Dittrich, Y. Gao, W. Nie, J. Cui, R. Chen, H. An, F. Fan, C. Li, Visualizing the Nano Cocatalyst Aligned Electric Fields on Single Photocatalyst Particles, *Nano Lett.* 17 (2017) 6735–6741. <https://doi.org/10.1021/acs.nanolett.7b02799>.
- [11] R. Asahi, T. Morikawa, T. Ohwaki, K. Aoki, Y. Taga, Visible-Light Photocatalysis in Nitrogen-Doped Titanium Oxides, *Science*. 293 (2001) 269–271. <https://doi.org/10.1126/science.1061051>.

- [12] C. Zhang, Y. Liu, J. Zhou, W. Jin, W. Chen, Tunability of **photocatalytic** selectivity of B-doped anatase TiO<sub>2</sub> microspheres in the visible light, *Dye. Pigment.* 156 (2018) 213–218.
- [13] H. Gong, Q. Liu, C. Huang, NiSe as an effective co-catalyst coupled with TiO<sub>2</sub> for enhanced photocatalytic hydrogen evolution, *Int. J. Hydrogen Energy.* 44 (2019) 4821–4831.  
<https://doi.org/https://doi.org/10.1016/j.ijhydene.2019.01.039>.
- [14] L.G.C. Rego, R. da Silva, J.A. Freire, R.C. Snoeberger, V.S. Batista, Visible Light Sensitization of TiO<sub>2</sub> Surfaces with Alq<sub>3</sub> Complexes, *J. Phys. Chem. C.* 114 (2010) 1317–1325. <https://doi.org/10.1021/jp9094479>.
- [15] S.N. Fedorov, V.Y. Bazhin, V.G. Povarov, Doping Titanium Dioxide by Fluoride Ion, *Mater. Sci. Forum.* 946 (2019) 181–185. <https://doi.org/10.4028/www.scientific.net/MSF.946.181>.
- [16] A. Fujishima, X. Zhang, D.A. Tryk, TiO<sub>2</sub> photocatalysis and related surface phenomena, *Surf. Sci. Rep.* 63 (2008) 515–582. <https://doi.org/https://doi.org/10.1016/j.surfrep.2008.10.001>.
- [17] A. Primo, A. Corma, H. García, Titania supported gold nanoparticles as photocatalyst, *Phys. Chem. Chem. Phys.* 13 (2011) 886–910. <https://doi.org/10.1039/C0CP00917B>.
- [18] D. Chen, S.H. Yoo, Q. Huang, G. Ali, S.O. Cho, Sonochemical Synthesis of Ag/AgCl Nanocubes and Their Efficient Visible-Light-Driven Photocatalytic Performance, *Chem. – A Eur. J.* 18 (2012) 5192–5200.  
<https://doi.org/https://doi.org/10.1002/chem.201103787>.
- [19] J. Liao, K. Zhang, L. Wang, W. Wang, Y. Wang, J. Xiao, L. Yu, Facile hydrothermal synthesis of heart-like Ag@AgCl with enhanced visible light photocatalytic performance, *Mater. Lett.* 83 (2012) 136–139.  
<https://doi.org/https://doi.org/10.1016/j.matlet.2012.06.017>.
- [20] P. Wang, B. Huang, Z. Lou, X. Zhang, X. Qin, Y. Dai, Z. Zheng, X. Wang, Synthesis of Highly Efficient Ag@AgCl Plasmonic Photocatalysts with Various Structures, *Chem. – A Eur. J.* 16 (2010) 538–544.  
<https://doi.org/https://doi.org/10.1002/chem.200901954>.
- [21] P. Wang, B. Huang, X. Qin, X. Zhang, Y. Dai, M.-H. Whangbo, Ag/AgBr/WO<sub>3</sub>·H<sub>2</sub>O: Visible-Light Photocatalyst for Bacteria Destruction, *Inorg. Chem.* 48 (2009) 10697–10702. <https://doi.org/10.1021/ic9014652>.
- [22] P. Wang, B. Huang, X. Zhang, X. Qin, H. Jin, Y. Dai, Z. Wang, J. Wei, J. Zhan, S. Wang, J. Wang, M.-H. Whangbo, Highly Efficient Visible-Light Plasmonic Photocatalyst Ag@AgBr, *Chem. – A Eur. J.* 15 (2009) 1821–1824. <https://doi.org/https://doi.org/10.1002/chem.200802327>.

Eliminato: photo-catalytic

- [23] S. Boufi, M. Abid, S. Bouattour, A.M. Ferraria, D.S. Conceição, L.F.V. Ferreira, G. Corbel, P.M. Neto, P.A. Lopes, M.R. Vilar, A.M.B. do Rego, Cotton functionalized with nanostructured TiO<sub>2</sub>-Ag-AgBr layer for solar photocatalytic degradation of dyes and toxic organophosphates, *Int. J. Biol. Macromol.* 128 (2019) 902–910. <https://doi.org/https://doi.org/10.1016/j.ijbiomac.2019.01.218>.
- [24] N. Bao, X. Miao, X. Hu, Q. Zhang, X. Jie, X. Zheng, Novel Synthesis of Plasmonic Ag/AgCl@TiO<sub>2</sub> Continuous Fibers with Enhanced Broadband Photocatalytic Performance, *Catal.* 7 (2017). <https://doi.org/10.3390/catal7040117>.
- [25] W. Liu, D. Chen, S.H. Yoo, S.O. Cho, Hierarchical visible-light-response Ag/AgCl@TiO<sub>2</sub> plasmonic photocatalysts for organic dye degradation, *Nanotechnology.* 24 (2013) 405706. <https://doi.org/10.1088/0957-4484/24/40/405706>.
- [26] Z.H. Shah, J. Wang, Y. Ge, C. Wang, W. Mao, S. Zhang, R. Lu, Highly enhanced plasmonic photocatalytic activity of Ag/AgCl/TiO<sub>2</sub> by CuO co-catalyst, *J. Mater. Chem. A.* 3 (2015) 3568–3575. <https://doi.org/10.1039/C4TA05777E>.
- [27] Q. Yang, M. Hu, J. Guo, Z. Ge, J. Feng, Synthesis and enhanced photocatalytic performance of Ag/AgCl/TiO<sub>2</sub> nanocomposites prepared by ion exchange method, *J. Mater.* 4 (2018) 402–411. <https://doi.org/https://doi.org/10.1016/j.jmat.2018.06.002>.
- [28] S. Basiri, A. Mehdinia, A. Jabbari, Biologically green synthesized silver nanoparticles as a facile and rapid label-free colorimetric probe for determination of Cu<sup>2+</sup> in water samples, *Spectrochim. Acta Part A Mol. Biomol. Spectrosc.* 171 (2017) 297–304. <https://doi.org/https://doi.org/10.1016/j.saa.2016.08.032>.
- [29] X. Chen, Y. Chen, L. Zou, X. Zhang, Y. Dong, J. Tang, D.J. McClements, W. Liu, Plant-Based Nanoparticles Prepared from Proteins and Phospholipids Consisting of a Core–Multilayer–Shell Structure: Fabrication, Stability, and Foamability, *J. Agric. Food Chem.* 67 (2019) 6574–6584. <https://doi.org/10.1021/acs.jafc.9b02028>.
- [30] S. Demirci, T. Dikici, M. Yurddaskal, S. Gultekin, M. Toparli, E. Celik, Synthesis and characterization of Ag doped TiO<sub>2</sub> heterojunction films and their photocatalytic performances, *Appl. Surf. Sci.* 390 (2016) 591–601. <https://doi.org/https://doi.org/10.1016/j.apsusc.2016.08.145>.

[31] N.U. Islam, K. Jalil, M. Shahid, A. Rauf, N. Muhammad, A. Khan, M.R. Shah, M.A. Khan, Green synthesis and biological activities of gold nanoparticles functionalized with *Salix alba*, Arab. J. Chem. 12 (2019) 2914–2925. <https://doi.org/https://doi.org/10.1016/j.arabjc.2015.06.025>.

[32] X. Lin, Y. Liang, Z. Lu, H. Lou, X. Zhang, S. Liu, B. Zheng, R. Liu, R. Fu, D. Wu, Mechanochemistry: A Green, Activation-Free and Top-Down Strategy to High-Surface-Area Carbon Materials, ACS Sustain. Chem. Eng. 5 (2017) 8535–8540. <https://doi.org/10.1021/acssuschemeng.7b02462>.

[33] K. Saravanakumar, R. Chelliah, S. Shanmugam, N.B. Varukattu, D.-H. Oh, K. Kathiresan, M.-H. Wang, Green synthesis and characterization of biologically active nanosilver from *Gardenia jasminoides* Ellis, J. Photochem seed extract. Photobiol. B Biol. 185 (2018) 126–135.

<https://doi.org/https://doi.org/10.1016/j.jphotobiol.2018.05.032>.

[34] X. Zhang, G. Parekh, B. Guo, X. Huang, Y. Dong, W. Han, X. Chen, G. Xiao, Polyphenol and self-assembly: metal polyphenol nanonetwork for drug delivery and pharmaceutical applications, Futur. Drug Discov. 1 (2019) FDD7. <https://doi.org/10.4155/fdd-2019-0001>.

[35] C. Dipankar, S. Murugan, The green synthesis, characterization and evaluation of the biological activities of silver nanoparticles synthesized from *Iresine herbstii* leaf aqueous extracts, Colloids Surfaces B Biointerfaces. 98 (2012) 112–119. <https://doi.org/https://doi.org/10.1016/j.colsurfb.2012.04.006>.

[36] N. Edayadulla, N. Basavegowda, Y.R. Lee, Green synthesis and characterization of palladium nanoparticles and their catalytic performance for the efficient synthesis of biologically interesting di(indolyl)indolin-2-ones, J. Ind. Eng. Chem. 21 (2015) 1365–1372. <https://doi.org/https://doi.org/10.1016/j.jiec.2014.06.007>.

[37] T. Pagar, S. Ghotekar, K. Pagar, S. Pansambal, R. Oza, A Review on Bio-Synthesized Co3O4 Nanoparticles using Plant Extracts and Their Diverse Applications, J. Chem. Rev. 1 (2019) 260–270. <https://doi.org/10.33945/SAMI/JCR.2019.4.2>.

[38] I. Rasaei, M. Ghannadnia, S. Baghshahi, Biosynthesis of silver nanoparticles using leaf extract of *Satureja hortensis* treated with NaCl and its antibacterial properties, Microporous Mesoporous Mater. 264 (2018) 240–247. <https://doi.org/https://doi.org/10.1016/j.micromeso.2018.01.032>.

Eliminato: seed extract of

- [39] J. Hadian, M. Hossein Mirjalili, M. Reza Kanani, A. Salehnia, P. Ganjipoor, Phytochemical and Morphological Characterization of *Satureja khuzistanica* Jamzad Populations from Iran, *Chem. Biodivers.* 8 (2011) 902–915. <https://doi.org/https://doi.org/10.1002/cbdv.201000249>.
- [40] M. Davoodi, A. Rustaiyan, S. Ebrahimi, Monoterpene Flavonoid from Aerial Parts of *Satureja khuzistanica*, *Rec. Nat. Prod.* 12 (2017) 175–178. <https://doi.org/10.25135/rnp.19.17.06.109>.
- [41] M. Malmir, A.R. Gohari, S. Saeidnia, O. Silva, A new bioactive monoterpene–flavonoid from *Satureja khuzistanica*, *Fitoterapia.* 105 (2015) 107–112. <https://doi.org/https://doi.org/10.1016/j.fitote.2015.06.012>.
- [42] F.M. Moghaddam, M.M. Farimani, S. Salahvarzi, G. Amin, Chemical Constituents of Dichloromethane Extract of Cultivated *Satureja khuzistanica*, *Evid. Based. Complement. Alternat. Med.* 4 (2007) 95–98. <https://doi.org/10.1093/ecam/nel065>.
- [43] Z. Ghasemi, V. Abdi, I. Sourinejad, Green fabrication of Ag/AgCl@TiO<sub>2</sub> superior plasmonic nanocomposite: Biosynthesis, characterization and photocatalytic activity under sunlight, *J. Alloys Compd.* 841 (2020) 155593. <https://doi.org/https://doi.org/10.1016/j.jallcom.2020.155593>.
- [44] M. Hussain, N.I. Raja, M. Iqbal, S. Aslam, Applications of Plant Flavonoids in the Green Synthesis of Colloidal Silver Nanoparticles and Impacts on Human Health, *Iran. J. Sci. Technol. Trans. A Sci.* 43 (2019) 1381–1392. <https://doi.org/10.1007/s40995-017-0431-6>.
- [45] P. Mulvaney, Surface Plasmon Spectroscopy of Nanosized Metal Particles, *Langmuir.* 12 (1996) 788–800. <https://doi.org/10.1021/la9502711>.
- [46] S.S. Momeni, M. Nasrollahzadeh, A. Rustaiyan, Green synthesis of the Cu/ZnO nanoparticles mediated by *Euphorbia prolifera* leaf extract and investigation of their catalytic activity, *J. Colloid Interface Sci.* 472 (2016) 173–179. <https://doi.org/https://doi.org/10.1016/j.jcis.2016.03.042>.
- [47] A. Nabikhan, K. Kandasamy, A. Raj, N.M. Alikunhi, Synthesis of antimicrobial silver nanoparticles by callus and leaf extracts from saltmarsh plant, *Sesuvium portulacastrum* L., *Colloids Surfaces B Biointerfaces.* 79 (2010) 488–493. <https://doi.org/https://doi.org/10.1016/j.colsurfb.2010.05.018>.
- [48] R. Atchudan, T.N.J.I. Edison, S. Perumal, R. Vinodh, Y.R. Lee, In-situ green synthesis of nitrogen-doped carbon dots for bioimaging and TiO<sub>2</sub> nanoparticles@nitrogen-doped carbon composite for photocatalytic

degradation of organic pollutants, *J. Alloys Compd.* 766 (2018) 12–24.

<https://doi.org/https://doi.org/10.1016/j.jallcom.2018.06.272>.

[49] T.N.J.I. Edison, R. Atchudan, J.-J. Shim, S. Kalimuthu, B.-C. Ahn, Y.R. Lee, Turn-off fluorescence sensor for the detection of ferric ion in water using green synthesized N-doped carbon dots and its bio-imaging, *J. Photochem. Photobiol. B Biol.* 158 (2016) 235–242. <https://doi.org/https://doi.org/10.1016/j.jphoto-biol.2016.03.010>.

[50] N. Muthuchamy, R. Atchudan, T.N.J.I. Edison, S. Perumal, Y.R. Lee, High-performance glucose biosensor based on green synthesized zinc oxide nanoparticle embedded nitrogen-doped carbon sheet, *J. Electroanal. Chem.* 816 (2018) 195–204. <https://doi.org/https://doi.org/10.1016/j.jelechem.2018.03.059>.

[51] C. Sarangapani, P. Lu, P. Behan, P. Bourke, P.J. Cullen, Humic acid and trihalomethane breakdown with potential by-product formations for atmospheric air plasma water treatment, *J. Ind. Eng. Chem.* 59 (2018) 350–361. <https://doi.org/https://doi.org/10.1016/j.jiec.2017.10.042>.

[52] M. Hudlikar, S. Joglekar, M. Dhaygude, K. Kodam, Green synthesis of TiO<sub>2</sub> nanoparticles by using aqueous extract of *Jatropha curcas* L. latex, *Mater. Lett.* 75 (2012) 196–199. <https://doi.org/https://doi.org/10.1016/j.matlet.2012.02.018>.

[53] T. Prasad, E.K. Elumalai, Biofabrication of Ag nanoparticles using *Moringa oleifera* leaf extract and their antimicrobial activity, *Asian Pac. J. Trop. Biomed.* 1 (2011) 439–442. [https://doi.org/https://doi.org/10.1016/S2221-1691\(11\)60096-8](https://doi.org/https://doi.org/10.1016/S2221-1691(11)60096-8).

[54] Z. Ghasemi, V. Abdi, I. Sourinejad, Single-step biosynthesis of Ag/AgCl@TiO<sub>2</sub> plasmonic nanocomposite with enhanced visible light photoactivity through aqueous leaf extract of a mangrove tree, *Appl. Nanosci.* 10 (2019) 507–516.

[55] A. Adamczyk, M. Rokita, The structural studies of Ag containing TiO<sub>2</sub>–SiO<sub>2</sub> gels and thin films deposited on steel, *J. Mol. Struct.* 1114 (2016) 171–180. <https://doi.org/https://doi.org/10.1016/j.mol-struc.2016.02.054>.

[56] Z. Wang, J. Chen, X. Hu, Preparation of nanocrystalline TiO<sub>2</sub> powders at near room temperature from peroxo-polytitanic acid gel, *Mater. Lett.* 43 (2000) 87–90. [https://doi.org/https://doi.org/10.1016/S0167-577X\(99\)00236-0](https://doi.org/https://doi.org/10.1016/S0167-577X(99)00236-0).

Formattato: Inglese (Stati Uniti)

Codice campo modificato

Formattato: Inglese (Stati Uniti)

Formattato: Inglese (Stati Uniti)

[57] [M. Al-Amin, S.C. Dey, T. U. Rashid, M. Ashaduzzaman, S.M. Shamsuddin, Solar assisted photocatalytic degradation of reactive azo dyes in presence of anatase titanium dioxide , Int. J. Latest Res. Eng. Technol. 2 \(2016\) 14-21.](#)

[58] Z. Ghasemi, H. Younesi, A.A. Zinatizadeh, Preparation, characterization and photocatalytic application of TiO<sub>2</sub>/Fe-ZSM-5 nanocomposite for the treatment of petroleum refinery wastewater: Optimization of process parameters by response surface methodology, *Chemosphere*. 159 (2016) 552–564.  
<https://doi.org/https://doi.org/10.1016/j.chemosphere.2016.06.058>.

[59] A. Peter, L. Mihaly-Cozmuta, A. Mihaly-Cozmuta, C. Nicula, C. Cadar, A. Jastrzębska, P. Kurtycz, A. Ol-szyna, A. Vulpoi, V. Danciu, T. Radu, L. Baia, Silver functionalized titania-silica xerogels: Preparation, mor-pho-structural and photocatalytic properties, kinetic modeling, *J. Alloys Compd.* 648 (2015) 890–902.  
<https://doi.org/https://doi.org/10.1016/j.jallcom.2015.07.022>.

[60] M. Gurulakshmi, M. Selvaraj, A. Selvamani, P. Vijayan, N.R. Sasi Rekha, K. Shanthi, Enhanced visible-light photocatalytic activity of V<sub>2</sub>O<sub>5</sub>/S-TiO<sub>2</sub> nanocomposites, *Appl. Catal. A Gen.* 449 (2012) 31–46.  
<https://doi.org/https://doi.org/10.1016/j.apcata.2012.09.039>.

[61] P. Wang, B. Huang, X. Qin, X. Zhang, Y. Dai, J. Wei, M.-H. Whangbo, Ag@AgCl: A Highly Efficient and Stable Photocatalyst Active under Visible Light, *Angew. Chemie Int. Ed.* 47 (2008) 7931–7933.  
<https://doi.org/https://doi.org/10.1002/anie.200802483>.

[62] Q. Xiang, J. Yu, B. Cheng, H.C. Ong, Microwave-Hydrothermal Preparation and Visible-Light Photoac-tivity of Plasmonic Photocatalyst Ag-TiO<sub>2</sub> Nanocomposite Hollow Spheres, *Chem. – An Asian J.* 5 (2010) 1466–1474. <https://doi.org/https://doi.org/10.1002/asia.200900695>.

[63] G. Calzaferrri, D. Brühwiler, S. Glaus, D. Schürch, A. Currao, C. Leiggenger, Quantum-sized silver, silver chloride and silver sulfide clusters, *J. Imaging Sci. Technol.* 45 (2001) 331–339.

[64] X. Wang, T.-T. Lim, Highly efficient and stable Ag–AgBr/TiO<sub>2</sub> composites for destruction of *Escherichia coli* under visible light irradiation, *Water Res.* 47 (2013) 4148–4158.  
<https://doi.org/https://doi.org/10.1016/j.watres.2012.11.057>.

**Spostato (inserimento) [1]**

**Formattato:** Colore carattere: Rosso

**Eliminato:** A. León, P. Reuquen, C. Garín, R. Segura, P. Vargas, P. Zapata, P.A.Orihuela, FTIR and Raman char-acterization of TiO<sub>2</sub> nanoparticles coated with polyeth-ylene glycol as carrier for 2-methoxyestradiol. *Applied Sciences*, 7(1) (2017).  
<https://doi.org/https://doi.org/49.10.3390/app7010049>

**Formattato:** Colore carattere: Rosso

[65] H. Xu, H. Li, J. Xia, S. Yin, Z. Luo, L. Liu, L. Xu, One-Pot Synthesis of Visible-Light-Driven Plasmonic Photocatalyst Ag/AgCl in Ionic Liquid, ACS Appl. Mater. Interfaces. 3 (2011) 22–29.

<https://doi.org/10.1021/am100781n>.

[66] X. Wang, Y. Tang, Z. Chen, T.-T. Lim, Highly stable heterostructured Ag–AgBr/TiO<sub>2</sub> composite: a bifunctional visible-light active photocatalyst for destruction of ibuprofen and bacteria, J. Mater. Chem. 22 (2012) 23149–23158. <https://doi.org/10.1039/C2JM35503E>.

[67] W. Li, R. Liang, A. Hu, Z. Huang, Y.N. Zhou, Generation of oxygen vacancies in visible light activated one-dimensional iodine TiO<sub>2</sub> photocatalysts, RSC Adv. 4 (2014) 36959–36966.

<https://doi.org/10.1039/C4RA04768K>.

[68] M.A. C., F. K. P., S. Singh, S. Baik, Hierarchically-structured silver nanoflowers for highly conductive metallic inks with dramatically reduced filler concentration, Sci. Rep. 6 (2016) 34894.

<https://doi.org/10.1038/srep34894>.

[69] S. Sumitha, S. Vasanthi, S. Shalini, S. V Chinni, S.C.B. Gopinath, P. Anbu, M.B. Bahari, R. Harish, S. Kathiresan, V. Ravichandran, Phyto-Mediated Photo Catalysed Green Synthesis of Silver Nanoparticles Using Durio Zibethinus Seed Extract: Antimicrobial and Cytotoxic Activity and Photocatalytic Applications, Mol. . 23 (2018). <https://doi.org/10.3390/molecules23123311>.

[70] P.D. Cozzoli, R. Comparelli, E. Fanizza, M.L. Curri, A. Agostiano, D. Laub, Photocatalytic Synthesis of Silver Nanoparticles Stabilized by TiO<sub>2</sub> Nanorods: A Semiconductor/Metal Nanocomposite in Homogeneous Nonpolar Solution, J. Am. Chem. Soc. 126 (2004) 3868–3879. <https://doi.org/10.1021/ja0395846>.

[71] H.M.M. Ibrahim, Green synthesis and characterization of silver nanoparticles using banana peel extract and their antimicrobial activity against representative microorganisms, J. Radiat. Res. Appl. Sci. 8 (2015) 265–275. <https://doi.org/https://doi.org/10.1016/j.jrras.2015.01.007>.

Spostato in su [1]: J.

Eliminato: [70] D. Li, R.B. Kaner, Shape and aggregation control of nanoparticles: Not shaken, not stirred,

Eliminato: Am. Chem. Soc. 128 (2006) 968–975. <https://doi.org/10.1021/ja056609n>.¶ [71]

Formattato: Colore carattere: Rosso

Eliminato: 72